Langmuir
Article
pubs.acs.org/Langmuir

Thorny Devil Nanotextured Fibers: The Way to Cooling Rates on the Order of 1 kW/cm^2

S. Sinha-Ray,[†] Y. Zhang,[†] and A. L. Yarin*[,†,‡]

[†]*Department of Mechanical and Industrial Engineering, University of Illinois at Chicago, 842 W. Taylor Street, Chicago Illinois 60607-7022, United States, and* [‡]*Center for Smart Interfaces, Technische Universität Darmstadt, Petersen str. 32, 64287 Darmstadt, Germany*

Received October 6, 2010. Revised Manuscript Received November 10, 2010

In the present work high-heat-flux surfaces, which should serve at temperatures of up to 200 °C, were covered by electrospun polymer nanofiber mats with thicknesses of about 30 μm. Then, four different metals were electroplated on separate polymer mats, namely, copper, silver, nickel, and gold. As a result, copper-plated nanofiber mats took on an appearance resembling that of a small Australian thorny devil lizard (i.e., they became very rough on the nanoscale) and acquired a high thermal diffusivity. Silver-plated nanofiber mats also became very rough because of the dendritelike and cactuslike nanostructures on their surfaces. However, nickel-plated nanofibers were only partially rough and their mats incorporated large domains of smooth nickel-plated fibers, and gold-plated nanofibers were practically smooth. Drop impacts on the hot surfaces coated with copper-plated and silver-plated nanofibers revealed tremendously high values of heat removal rates of up to 0.6 kW/cm^2. Such high values of heat flux are more than an order of magnitude higher that the currently available ones and probably can be increased even more using the same technique. They open some intriguing perspectives for the cooling of high-heat-flux microelectronics and optoelectronics and for further miniaturization of such devices, especially for such applications as UAVs and UGVs.

1. Introduction

Cooling high-heat-flux surfaces stems from severe restrictions imposed on microelectronics, optoelectronics, and radiological devices by an increase in heat release associated with further miniaturization. The situation becomes extremely acute in robotic devices such as unmanned aerial vehicles and unmanned ground vehicles (UAVs and UGVs, respectively). In particular, carrying electro-optical, infrared, and other sensors, video equipment, targeting systems and running signal intelligence systems or real-time image processing promote an endless appetite for UAVs with greater power densities on board.[1−3] Drop and spray cooling in such situations represent a desirable and in some cases the only possible remedy.[1−4] Indeed, spray cooling is one of the most effective and aggressive methods of cooling compared to other air- or liquid-cooling systems.[1−5] It was discovered recently that the efficiency of spray cooling can be enhanced still more if a high-heat-flux surface is covered with a nanotextured layer, namely, an electrospun polymer nanofiber mat with a thickness of about 100 μm.[6] Such an approach where a hot surface is cooled more effectively through a "furry overcoat", almost 90−95% of which is filled with air, is rather paradoxical. It triggered a deeper fluid mechanical study in the following work,[7] where it was shown that the texture of the electrospun nanofiber mats facilitates the penetration of water into their pores and simultaneously prevents the receding motion of the contact line of spread-out drops and eliminates bouncing. All of these phenomena are greatly beneficial to spray cooling through nanofiber mats.

However, polymer nanofibers have a relatively low thermal diffusivity of their own, and the individual fibers are fairly smooth. Therefore, a further enhancement of spray cooling through nanofiber mats might probably be achieved if they would be metalized and made as rough as possible as a means to increase the effective surface area of nanofiber-coated hot surfaces further. In this context, our attention in this work is directed to the electroplating of electrospun nanofiber mats deposited on high-heat-flux surfaces to facilitate their cooling.

Electroplating is a process that coats conductive or semiconductive objects with a thin metal layer. The process uses an electrical current to reduce cations of a desired metal from a solution. It is used to deposit various metals on targeted surfaces.[8,9] The process is technologically stable and attractive for growing thin films and/or nanostructures with potentially superior thermoelectric and microelectronic properties.[10,11] There is a significant body of research on electroplating and many examples of its successful application in the microelectronics, automotive, and aerospace industries.[12−15] However, studies on the electroplating of

*To whom correspondence should be addressed. E-mail: ayarin@uic.edu. Phone: +1(312) 996-3472. Fax: +1(312) 413-0447.

(1) Child, J. *COTS J.* (*J. Military Electron. Comput.*) **2009**, *2*, 1.
(2) Kinney, D. *COTS J.* (*J. Military Electron. Comput.*) **2009**, *2*, 3.
(3) Mudawar, I. *IEEE Trans. Compon. Packag. Technol.* **2001**, *24*, 122.
(4) Briones, A. M.; Ervin, J. S.; Putnam, S. A.; Byrd, L. W.; Gschwender, L. *Langmuir* **2010**, *26*, 13272.
(5) Yarin, L. P.; Mosyak, A.; Hetsroni, G. *Fluid Flow, Heat Transfer and Boiling in Micro-Channels*; Springer: Berlin, 2009.
(6) Srikar, R.; Gambaryan-Roisman, T.; Steffes, C.; Stephan, P.; Tropea, C.; Yarin, A. L. *Int. J. Heat Mass Transfer* **2009**, *52*, 5814.
(7) Lembach, A.; Tan, H. B.; Roisman, I. V.; Gambaryan-Roisman, T.; Zhang, Y.; Tropea, C.; Yarin, A. L. *Langmuir* **2010**, *26*, 9516.
(8) Schlesinger, M.; Paunovic, M. *Modern Electroplating*, 4th ed.; Wiley: New York, 2000.
(9) Graham, A. K. *Electroplating Engineering Handbook*, 3rd ed.; VNR: New York, 1971.
(10) Feng, Q. Y.; Li, T. J.; Zhang, Z. T.; Zhang, J.; Liu, M.; Jin, J. Z. *Surf. Coat. Technol.* **2007**, *201*, 6247.
(11) Li, H.; Wan, Y.; Liang, H.; Li, X.; Huang, Y.; He, F. *Appl. Surf. Sci.* **2009**, *256*, 1614.
(12) Sikder, A. K.; Misra, D. S.; Singhbal, D.; Chakravorty, S. *Surf. Coat. Technol.* **1999**, *114*, 230.
(13) Aruna, S. T.; Diwakar, S.; Jain, A.; Rajam, K. S. *Surf. Eng.* **2005**, *21*, 209.
(14) Xu, R. D.; Wang, J. L.; He, L. F.; Guo, Z. C. *Surf. Coat. Technol.* **2008**, *202*, 1574.

metal coatings on nanotextured nonconductive polymer nanofibers are scarce.[16−18]

In the present work, the electrospun nanofiber mats were made metallic using electroplating. Then, their cooling capabilities in the case of drop cooling were studied, which revealed heat removal rates of up to 0.6 kW/cm^2. The experimental results on the rate of drop evaporation inside metallic nanofiber mats are also supported by the theoretical estimates.

2. Experimental Section: Materials and Methods

2.1. Fabrication of Metal-Plated Nanofiber Mats.

2.1.1. Materials. Polyacylonitrile (PAN, $M_w = 150$ kDa) was obtained from Polymer Inc. *N*-Dimethyl formamide (DMF) anhydrous 99.8%, sulfuric acid, hydrochloric acid, copper sulfate, formaldehyde, silver nitrate, potassium hydroxide, ammonium hydroxide, nitric acid, nickel sulfamate, boracic acid, sodium hydroxide, triammonium citrate, potassium aurochlorate, and sodium sulfite were obtained from Sigma-Aldrich. Copper plates obtained from McMaster-Carr were cut into 1 × 1 in.^{2} pieces and used as substrates. The substrates were cleaned with acetone by sonication prior to use.

2.1.2. Preparation of Solutions. For electrospinning, a 12 wt % PAN solution in DMF was prepared. For electroplating, the solutions were prepared as follows: (i) For electroplating copper, sulfuric acid (5 g), hydrochloric acid (0.5 g), copper sulfate (16 g), and formaldehyde (10 g) were mixed with 100 mL of deionized (DI) water to prepare a copper plating solution. (ii) For electroplating silver, silver nitrate, (0.5 g) and potassium hydroxide (0.25 g) were mixed with 5 mL of DI water separately. Then these two solutions were mixed with ammonium hydroxide (1.25 mL) to prepare solution A. Sugar (2.25 g), nitric acid (0.1 mL), and 25 mL of DI water were mixed and boiled to prepare solution B. Then, solution A and cooled solution B were mixed before the silver plating process was started. (iii) For electroplating nickel, nickel sulfamate (40 g) and boracic acid (3 g) were mixed with 100 mL of DI water. Then the solution pH was adjusted to 4.5 by adding the proper amount of sodium hydroxide solution. (iv) For electroplating gold, triammonium citrate (10 g) and potassium aurochlorate ($KAuCl_4$, 0.25 g) were mixed with 50 mL of DI water. The solution was stirred until the potassium aurochlorate salt was fully dissolved. Then, sodium sulfite (3 g) was added to the solution. The initially opaque solution became transparent after the addition of sodium sulfite.

2.1.3. Electrospinning and Sensitization of Polymer Nanofiber Mats. Polymer nanofiber mats were prepared by electrospinning a PAN solution using a standard electrospinning setup described elsewhere.[19−21] Randomly oriented nanofibers were collected on thin copper substrates. Fibers were electrospun onto copper substrates for 5−7 min while keeping the flow rate at 0.8 mL/h and the electric field at about 1 kV/cm, which resulted in nanofiber thicknesses on the order of 20−30 μm. The nanofiber mats adhered to the copper substrates and were used as templates for further electroplating.

For electroplating, the nanofiber mats had to be sensitized to make them conducting. For that purpose, the nanofiber mats were sputter coated with Pt−Pd to a thickness of 15 nm by using a Cressington sputter controller.

2.1.4. Electroplating. For electroplating, the sputter-coated nanofiber mats were immersed in one of the above-mentioned solutions (i−iv) and served as a cathode. A bare copper substrate served as an anode. An EPS-10 laboratory electroplating station (model 2009) with a cathode rotating stand was used to electroplate nanofiber mats.

2.1.5. Electroplating of Copper. For copper plating, the electric current density was kept at 100 mA/cm^2 for 3 min to form a fine coating. Then, the electroplated sample was taken out of the electroplating bath. After that, the copper-plated nanofiber mat was immersed into 10% formaldehyde solution for 5 min and then rinsed twice with DI water. It is emphasized that the copper-plated nanofiber mat was copper bonded to the copper substrate. More details on the electroplating of copper on nanofibers can be found in Appendix I.

2.1.6. Electroplating of Silver. For silver plating, the electric current density was kept at 100−150 mA/cm^2 for 5 min and then the sample was taken out of the electroplating bath. Then, the silver-plated nanofiber mat was immersed into 10% formaldehyde solution for 5 min and rinsed twice with DI water. Because the nanofiber mat was deposited on the copper substrate, the copper−silver bonds formed here are weaker than the copper−copper bonds formed in the copper-plating experiments. That is caused by differences in the metal crystal structures as well as in the electrochemical potentials of different metals. More details on the electroplating of silver on nanofibers can be found in Appendix II.

2.1.7. Electroplating of Nickel. For nickel plating, the electric current density was kept at 50 mA/cm^2 for 5 min and then the sample was taken out of the electroplating bath. Then, the nickel-plated nanofiber mat was immersed in 10% formaldehyde solution for 5 min and rinsed twice with DI water. The nickel−copper bonds formed here are weaker than the copper−copper bonds formed in the copper-plating experiment, similar to the situation mentioned above. More details on the electroplating of nickel on nanofibers can be found in Appendix III.

2.1.8. Electroplating of Gold. For gold plating, the electric current density was kept at around 50 mA/cm^2 for 10 min and then the sample was taken out of the electroplating bath. Then, the gold-plated nanofiber mat was immersed in 10% formaldehyde solution for 5 min and rinsed twice with DI water. The gold−copper bonds formed here are weaker than the copper−copper bonds formed in the copper plating experiment, similar to the situation mentioned above. More details on the electroplating of gold on nanofibers can be found in Appendix IV.

2.1.9. Roughness Control. The nucleation and crystal growth modes of metal electrodeposits play a significant role in the development of nanotexture. When the nucleation rate is higher than the crystal growth rate, a smooth metal coating will be obtained. However, if the crystal growth rate appears to be faster than the nucleation rate, then a rough metal surface can be obtained. There are many ways to control the nucleation and crystal growth rates. This can be achieved, for example, by decreasing the rate of chemical reaction, which can be done by decreasing the reactant concentrations, controlling the temperature of the system, forming specific intermediates during electroplating, and so on. As a result of decreasing the rate of chemical reaction, the nucleation rate can be slowed down, and by increasing the electric current density, the crystal growth rate can be increased correspondingly.

2.1.10. Electron Microscopy. All scanning electron microscopy of metal-plated nanofiber mats was done using a JEOL JSM-6320F with a cold emission source.

2.2. Experiments with Drop Impact on Hot Nanotextured Surfaces.

2.2.1. Drop Impact Experiments. For the investigation of drop impacts, three different variants of the experimental setup depicted in Figure 1 were used. In this setup, substrates were kept on a hot plate at a constant temperature. Water was supplied to the needle end using a syringe pump. As a result, a single drop had been growing at the needle edge and then disconnected and dripped because of gravity. After that, the pump had been

(15) Vaezi, M. R.; Sadrnezhaad, S. K.; Nikzad, L. *Colloids Surf., A* **2008**, *315*, 176.
(16) Pinto, N. J.; Carrion, P.; Quinones, J. X. *Mater. Sci. Eng., A* **2004**, *366*, 1.
(17) Ochanda, F.; Jones, W. E. *Langmuir* **2005**, *21*, 10791.
(18) Ochanda, F.; Jones, W. E. *Langmuir* **2007**, *23*, 795.
(19) Reneker, D. H.; Yarin, A. L.; Fong, H.; Koombhongse, S. *J. Appl. Phys.* **2000**, *87*, 4531.
(20) Reneker, D. H.; Yarin, A. L.; Zussman, E.; Xu, H. *Adv. Appl. Mech.* **2007**, *41*, 43.
(21) Reneker, D. H.; Yarin, A. L. *Polymer* **2008**, *49*, 2387.

stopped. Water drops were dripped from a height that could be varied. For the visualization of drop impacts on metal-plated nanofiber mats, two cameras were used in the basic setup in Figure 1. For high-speed photography, a Redlake Motion Pro camera was used at a recording speed of 2000 fps, and for capturing top views, an ordinary Pulnix 7 M CCD video camera at a recording speed of 30 fps was used. In the second variant of the setup, the low-speed CCD camera was removed and only the high-speed CCD camera was used. In the third variant of the setup, only the low-speed CCD camera was used.

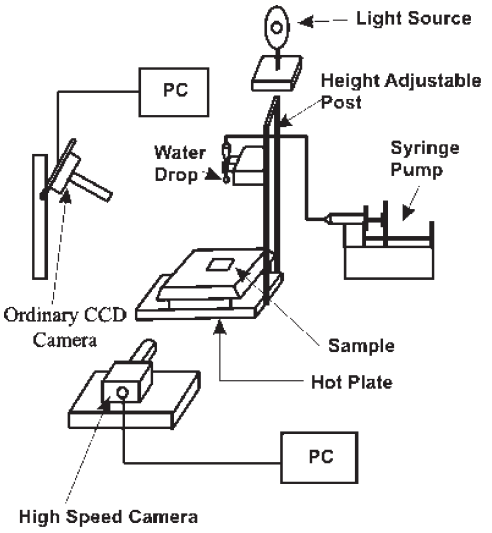

Figure 1. Schematic of the experimental setup.

Table 1. Sample Temperature versus Display Temperature

display temperature (°C)	sample temperature (°C)
40	34
50	41
60	50.3
70	57.5
80	68.4
90	73.6
100	83.7
110	93.5
125	102.7
150	125.6
200	172.2

2.2.2. Calibration of Temperature on a Hot Plate. It is emphasized that the temperature on the display of the hot plate is not exactly the same as that of the sample on top of it. Therefore, measurements of the sample temperature were made separately and the calibration of the temperature versus that of the display is shown in Table 1. The thin copper substrates used in this work were covered by metal-plated nanofiber mats with thicknesses of about 30 μm. In this case, the substrate steady-state temperature distribution is uniform and accurately represented by its base temperature measured by a thermocouple. The latter represents the sample temperature (including nanofibers) given in Table 1.

3. Experimental Observations

3.1. Metal-Plated Nanofiber Mats. SEM images of the electroplated nanofiber mats are shown in Figures 2−5. The individual copper-plated fibers possess thorny (Figure 2c) and grainy (Figure 2d) nanotexture, which makes them reminiscent of Australian thorny devil lizards. Silver-plated nanofibers are equally rough but show predominantly dendritelike or cactuslike structure (Figure 3). Nickel-plated nanofibers reveal an additional type of nanotexture, namely, the distinct domains of smooth and rough fibers (Figure 4). In contrast to the other cases, gold-plated fibers are smoother and possess only infrequent spheroidal appendices or their small clusters (Figure 5). A comparison of the images with the same magnification (Figures 2c,d, 3c,d, 4c,d, and 5c,d) shows that copper-plated fibers uniformly possess the roughest nanotexture. Moreover, even though only the upper layer of the nanofibers appears to be rough in Figures 2 and 3, this is an artifact related to electron beam focusing in SEM. The images of a cut

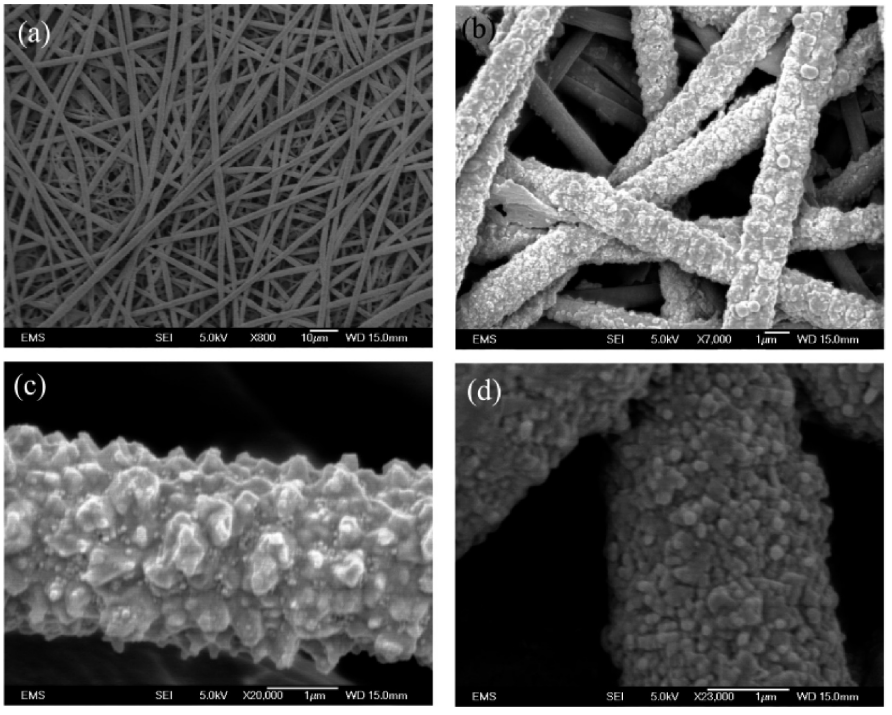

Figure 2. SEM images of the thorny devil copper-plated fibers. (a) Overall view of the copper-plated fiber mat. (b) Enlarged view of the top layer. Individual fibers at different locations: (c) thorny and (d) grainy nanotextures.

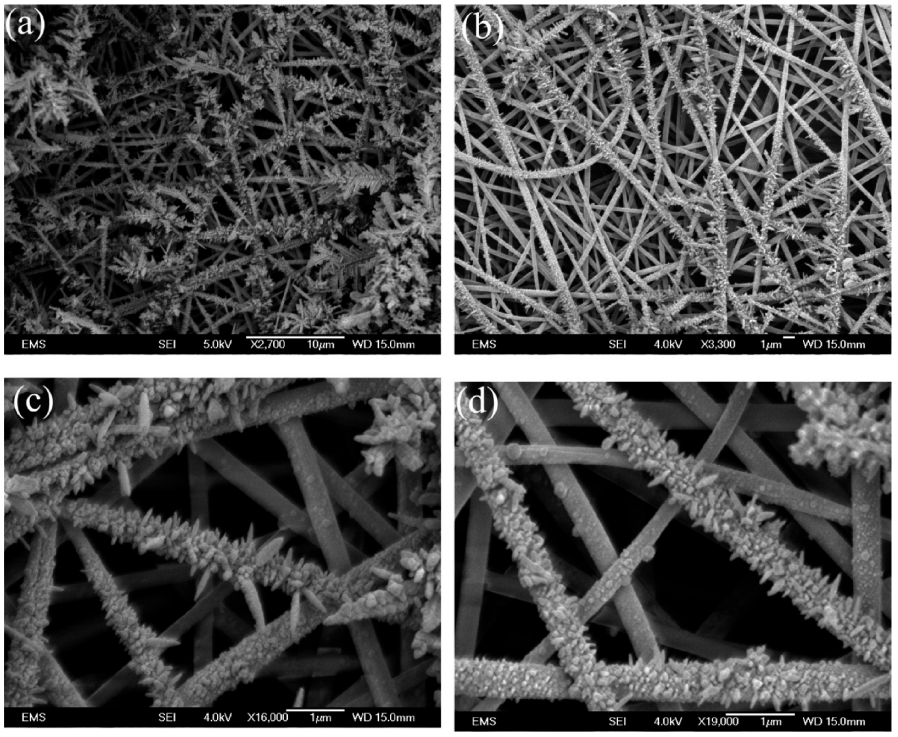

Figure 3. SEM images of the dendritelike and cactuslike silver-plated nanofiber mats. (a, b) Overall view of the silver-plated nanofiber mat at two different locations. The fibers look like dendrites or fern leaves (a) or are more cactuslike (b). (c, d) Cactuslike nanofibers shown in more detail.

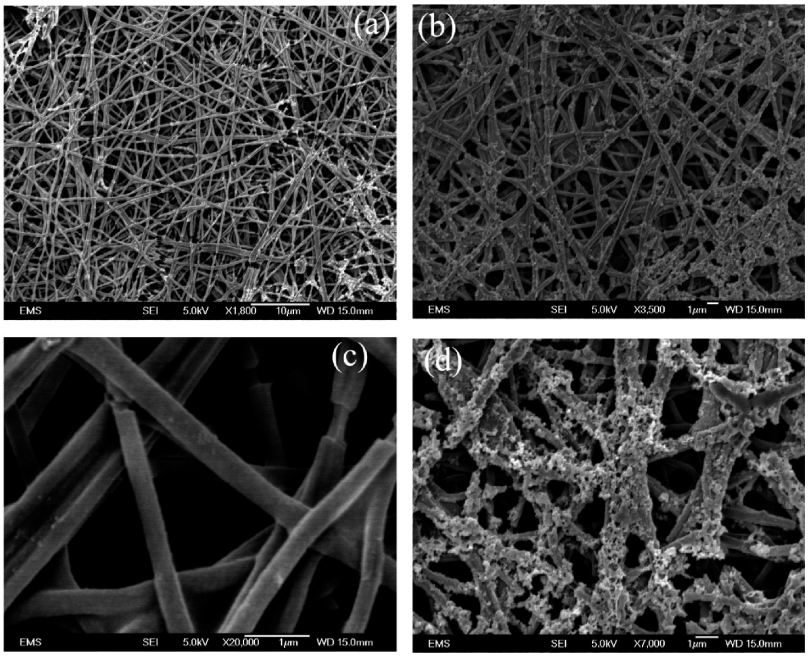

Figure 4. SEM images of nickel-plated nanofibers. (a, b) Overall view of nickel-plated nanofibers at two different locations. (c) Smooth nanotexture of the individual nickel-plated nanofibers. In some places, the coating broke because of rough handling, exposing the skeletal-template polymer. (d) Rough nanotexture of the individual nickel-plated nanofibers.

copper-plated nanofiber mat in Figure 6 show that the fibers on the bottom of the mat in contact with the underlying substrate are as thorny-devil-like as those near the surface of the mat in Figure 2. Therefore, the fibers are rough throughout the whole mat depth.

Similarly, the nickel-plated fibers possess a mosaic of smooth and rough domains, and gold-plated fibers are practically smooth throughout the mat depth. The nucleation and crystal growth modes of metal electrodeposits have a vital bearing on the development of nanotexture. Generally speaking, when nucleation is faster than crystal growth, a smooth coating will be obtained. The nucleation rate depends on a number of factors, such as the rate of chemical reaction, the temperature, the initial metallurgical state of the cathode, and so forth. For gold plating, the formation of $[Au(SO_3)_2]^{3-}$ complexes makes the cathode polarization rate slower, which means that the nucleation is faster than the crystal growth. However, for copper and nickel,

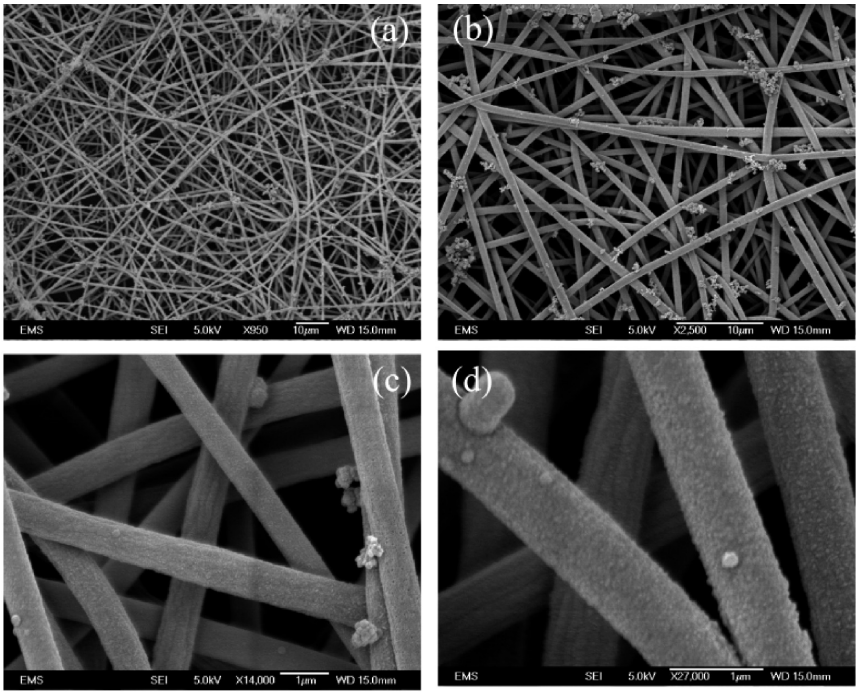

Figure 5. SEM images of gold-plated nanofibers. (a) Overall view of the gold-plated nanofiber mat. (b) Enlarged view of the upper layers with the visible appendices scattered over the fibers. (c, d) Several individual fibers: almost smooth coatings with some appendices at two different locations.

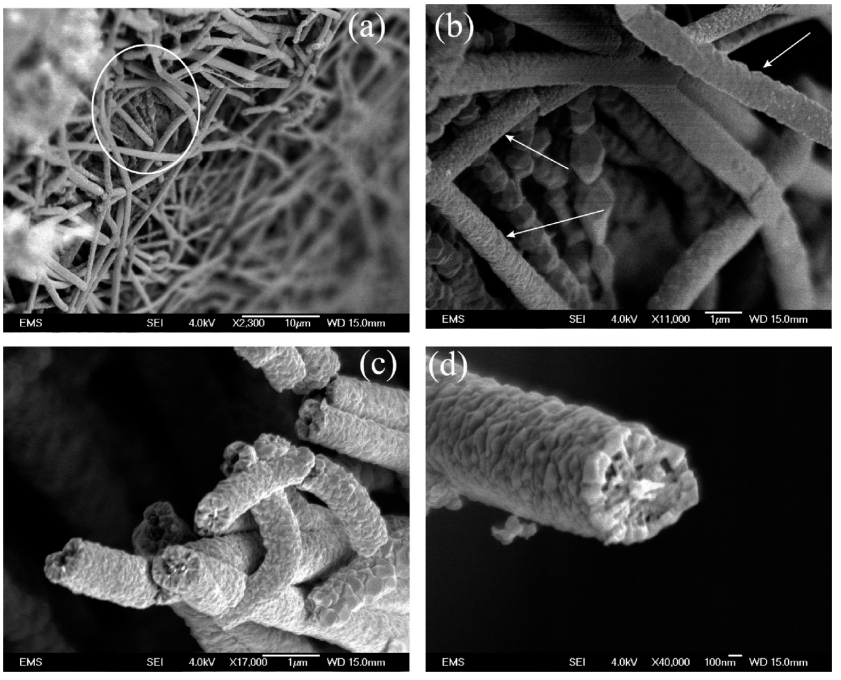

Figure 6. SEM images of a cut copper-plated nanofiber mat. (a) Overall view of the cut mat near the underlying substrate. The encircled area seemingly shows that some copper-plated nanofibers are rough, whereas some others seem to be smooth. The latter is just an artifact because these smoothlike nanofibers are just out of focus. (b) Indeed, the enlarged image of the encircled area in panel a shows that the previously "smooth" nanofibers indicated by arrows in reality have a rough structure as well. (c, d) Detailed structure of the copper-plated fiber mat near the substrate in another place.

the reaction is "simple" and fast, which may lead to a higher cathode polarization speed and thus a faster nucleation speed. In the case of the gold-plated nanofibers in Figure 5, the formation of the visibly rough domains can be attributed to the high speed of the outward crystal growth of the deposit by continuous nucleation during the last step of the 3D metal electrodeposition. In general, if the crystal growth is faster than the nucleation rate, then one can obtain a rough surface, which is a desirable feature in the present work.

3.2. Surface Enhancement Factor. The surface enhancement factor α is defined as the ratio of the overall surface area including that of the fibers on a unit area of a substrate to that of

Table 2. Surface Enhancement Factor α for Various Sample Temperatures

temperature (°C) display/sample	Δt_1 (s)	Δt_2 (s)	$\Delta t_1/\Delta t_2$	S_1/S_{20}	α	relative surface area of nanofibers, $\Delta S/S_{20}$
40/34	255	30	8.5	0.873	7.42	6.42
50/41	195	21	9.3	0.852	7.91	6.91
60/50.3	100	18	5.56	0.933	5.18	4.18
70/57.5	60	15	4	0.804	3.22	2.22
80/68.4	39	13	3	0.833	2.50	1.50
90/73.6	25	9	2.78	0.717	1.99	0.99
100/83.7	18	7	2.57	0.934	2.40	1.40
110/93.5	16	5	3.2	0.908	2.90	1.90

the bare substrate. It is emphasized that in the general case the bare substrate used for comparison might be made of a different metal than the one coated with nanofibers because in the experiments described in the present section the expectation is that the surface enhancement factor is a pure geometric parameter. For the evaluation of the surface enhancement factor, the following experiment was conducted. A drop of water was released from a fixed height of 10.64 cm onto either a bare copper substrate or a copper substrate covered with a copper-plated nanofiber mat. The bare substrate and the fiber-mat-coated substrate were kept at the same fixed temperature when drop evaporation was observed. In different experiments, a fixed temperature was chosen from the range from 40 to 110 °C (the display temperature, which corresponds to a 34 to 93.5 °C sample temperature) with a 10 °C step (the display temperature). The evaporation time Δt of water drops was recorded using an ordinary CCD camera. The thermal balances for a bare substrate and a nanofiber-coated substrate are

$$LV_1 = \frac{k_{w_1}}{\delta_{w_1}} \Delta T S_1 \Delta t_1 \quad (1)$$

$$LV_2 = \frac{k_{w_2}}{\delta_{w_2}} \Delta T S_2 \Delta t_2 \quad (2)$$

where subscripts 1 and 2 refer to a bare substrate and a nanofiber-coated substrate, respectively. Also, L is the latent heat of evaporation, V is the drop volume, k_w and δ_w are the thermal conductivity and thickness of a substrate, respectively, S is the wetted surface area, and ΔT is the excess temperature of the substrates relative to room temperature.

Area S_2 can be represented as the sum of the wetted substrate area S_{20} and the wetted nanofiber area on the substrate ΔS

$$S_2 = S_{20} + \Delta S \quad (3)$$

In the experiments, it was $k_{w_1} = k_{w_2}$ and $\delta_{w_1} = \delta_{w_2}$ (i.e., two substrates of the same material and thickness were used). Also, two drops were identical (i.e., $V_1 = V_2 = 3.053$ mm^3, which corresponds to an initial drop radius of 0.9 mm.) Then, eqs 1−3 reduce to

$$\alpha = 1 + \frac{\Delta S}{S_{20}} = \frac{\Delta t_1}{\Delta t_2} \frac{S_1}{S_{20}} \quad (4)$$

The values of Δt_1, Δt_2, and S_1/S_{20} measured experimentally are listed in Table 2 together with the surface enhancement factor α found from eq 4. The relative surface area of the nanofibers was determined from eq 4 to be

$$\frac{\Delta S}{S_{20}} = \alpha - 1 \quad (5)$$

which is also presented in Table 2.

It is emphasized that the experimental data in Table 2 fully support eqs 1 and 2. Indeed, taking for room temperature the value of 20 °C and taking the sample temperature from Table 1,

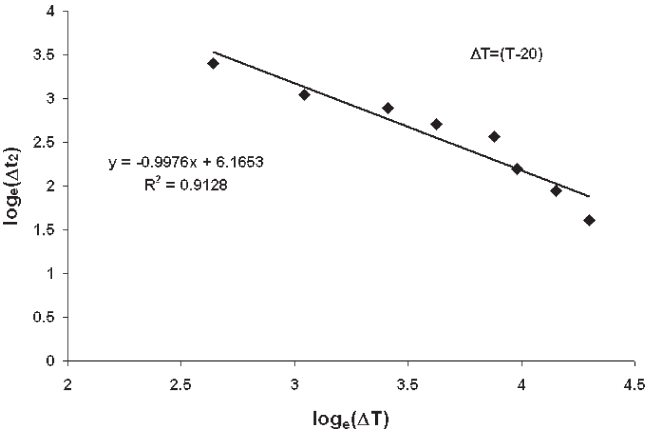

Figure 7. Dependence of the drop evaporation time on a metal-plated nanofiber mat on ΔT at a room temperature of 20 °C. The slope is equal to −0.9976 in log−log coordinates; from eq 2, a slope of −1 is anticipated. The coefficient of determination is $R^2 = 0.9128$.

one can plot the measured value of the evaporation time on metal-plated nanofiber mats Δt_2 versus ΔT. The result plotted in Figure 7 fully supports the linear dependence of Δt_2 on ΔT^{-1} as anticipated from eq 2.

The data in Table 2 and Figure 7 show that at elevated temperatures the linear dependence of Δt_2 on ΔT^{-1} deteriorates and the effective value of α decreases, which probably can be attributed to the effect of rapid evaporation and boiling inside the copper-plated nanofiber mat. Therefore, only the values at the two lowest temperatures are relevant to the determination of such a purely geometric parameter as the surface enhancement factor α. Then, the surface enhancement factor due to the presence of nanofibers is in the range of $\alpha \approx 7.5-8$.

3.3. Morphology of Drop Impact Cooling through Copper-Plated Mats. Copper substrates coated with metal-plated nanofiber mats and bare copper uncoated substrates used for control were located on a hot plate at different fixed elevated temperatures. Water drops released from different heights were used locally to cool them to evaluate the corresponding cooling rate. In these experiments, the setup depicted in Figure 1 was initially employed. A substrate coated with a copper-plated nanofiber mat was placed on a hot plate at a fixed temperature of 150 °C (the display temperature corresponding to 125.6 °C for the sample). A single water drop of radius $a_0 = 0.9$ mm was dripped from various heights. The whole process (drop approach, spreading, and evaporation at the nanofiber mat) was captured simultaneously with an ordinary CCD camera (recording at 30 fps) and a high-speed camera (at 2000 fps). The ordinary CCD camera recorded the process from the top whereas the high-speed camera recorded the process from the side. Drops fell onto nanofiber mats from heights of $h = 3.55$, 6.15, 8.75, 11.15, 13.75, and 17.95 cm, which correspond to impact velocities of $V_0 = 83.46$, 109.85,

131.02, 147.91, 164.25, and 187.66 cm/s, respectively (evaluated as $V_0 = (2gh)^{1/2}$, where g is the acceleration due to gravity).

The top- and side-view images of drop impact from a height of 3.55 cm, with spreading and evaporation on a copper-plated nanofiber mat, are shown in Figures 8 and 9, respectively. Figure 8a depicts the moment of drop impact ($t = 0$) on the nanofiber surface. Figure 8b shows that at $t = 32.5$ ms water boiling is visible on the surface, whereas Figure 8c demonstrates that boiling seemingly ceases at $t = 66$ ms and there is no longer any visible activity on the surface. In panel a in Figure 9, the area surrounded by the white tracing contour corresponds to the projection of the oncoming drop onto the nanofiber mat surface. This image corresponds approximately to the top view of the situation similar to that in Figure 8a. In panel b in Figure 9, the area surrounded by the white tracing contour is still covered with water, which is visible in the side view of corresponding Figure 8b. Water was either partially evaporated or penetrated into the copper-plated mat between the images in Figure 9a,b. In panel c in Figure 9, the area surrounded by the white tracing contour is still wetted, even though active boiling on the surface and probably inside the mat has already ended according to corresponding Figure 8c. From that time on, the wetted area rapidly begins to lose its visible contrast, which ultimately corresponds to drying. It should be mentioned that when the images recorded with the CCD camera for longer times were analyzed, some minor contrast variations were observed in the next four to five frames, which corresponds to $t = 132-165$ ms. However, the contrast variation was so small that no visible activity was recorded by the high-speed camera in this time range. Therefore, it was concluded that the above-mentioned minor contrast variations most probably resulted from the condensation of water vapor onto the nanofiber mat, which followed the cessation of the cooling stage. Because of the low time resolution of the CCD camera used, it could not resolve the time frame of $t < 33$ ms in Figure 9. However, Figure 9 shows that the water drop impacted the surface between panels a and b in Figure 9, which corresponds to $0 \leq t \leq 33$ ms, and that it fully evaporated sometime after panel c, which corresponds to $66 \leq t \leq 99$ ms. However, Figure 8 shows that the activity on the surface of the nanofiber mat ceased at 66 ms, which is close to the time frame suggested by Figure 9. Similar observations were made for drop impacts from other heights.

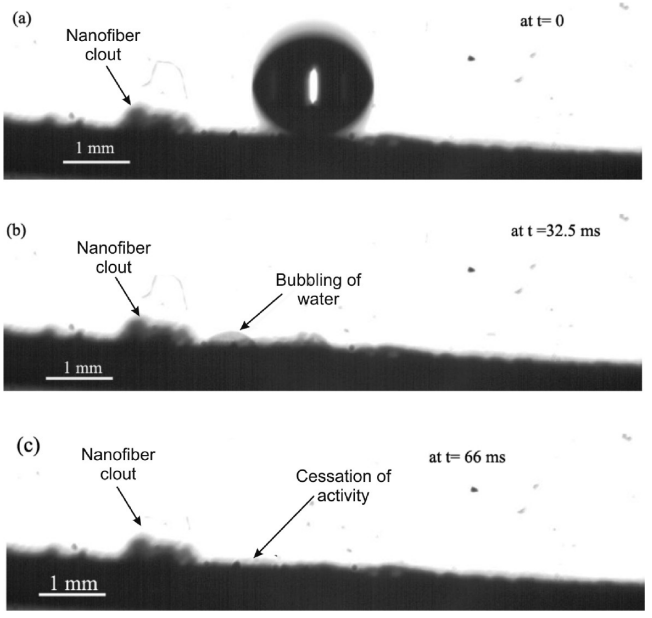

Figure 8. Drop impact from a height of 3.55 cm ($V_0 = 83.46$ cm/s) onto a copper-plated nanofiber mat at 150 °C (the display temperature corresponding to 125.6 °C for the sample). (a) 0 ms at the moment of impact, (b) 32.5 ms, and (c) 66 ms.

3.4. Cooling Rates with Copper-Plated Nanofiber Mats. As in ref 6, the heat flux j was evaluated from the experimental data using the following expression: $j = \rho(4\pi a_0^3/3)(1 - p)L/\pi a^2 \Delta t$, where ρ is the liquid density, a_0 the initial drop radius, a is the maximum spread-out radius after drop impact onto the nanofiber mat, L is the latent heat of evaporation of water, and Δt is the duration of drop evaporation. The above expression also involves the "atomization" volume ratio p. The value of p corresponds to mass lost due to atomization from the mat surface, which accompanied the evaporation process in some cases. The

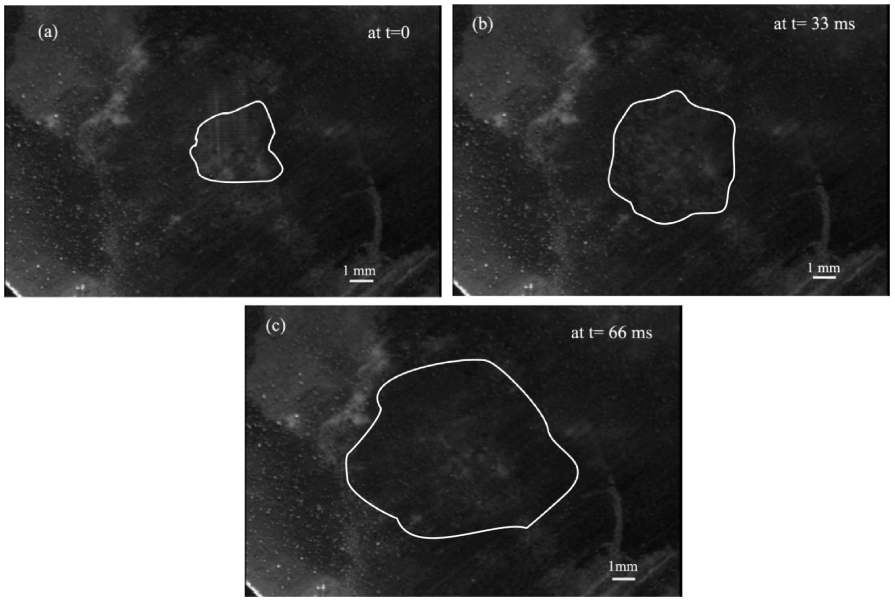

Figure 9. Top view of the drop impact onto a copper-plated nanofiber mat corresponding to that of Figure 7 (at 150 °C, the display temperature corresponding to 125.6 °C for the sample). (a) $t = 0$ ms, (b) $t = 33$ ms (the closest to 32.5 ms in Figure 8b that the ordinary CCD could resolve), and (c) t = 66 ms.

Table 3. Maximum Drop Spread Factor and Cooling Rates Corresponding to Water Drop Impact on Copper-Plated Nanofiber Mats at 150 °C[a]

h (cm)	V_0 (cm/s)	Δt (ms)	ξ	p	j (kW/cm^2)
3.55	83.46	66	2.6	0	0.607
6.15	109.85	58	2.85	0	0.575
8.75	131.02	53.5	3.02	0	0.555
11.15	147.91	52.5	3.15	0	0.521
13.75	164.25	47	3.25	0	0.543

[a] The display temperature corresponding to 125.6 °C of the sample. No visible atomization was recorded; therefore, $p = 0$.

direct measurements of p are discussed below. Using the side-view images, it is practically impossible to resolve the spread-out radius a. The top-view images showed that the maximum spread factor $\xi = a/a_0$ for water drops on the copper-plated mats was close to 2. Then, the values of the spread-out radius a (and thus ξ) were evaluated using the following widely used expression:[22,23] $\xi = 0.61(We/Oh)^{0.166}$, where the Weber and Ohnesorge numbers are defined as $We = \rho 2a_0 V_0^2/\sigma$ and $Oh = \mu/(\rho\sigma 2a_0)^{1/2}$, with μ and σ being the viscosity and surface tension of water. Such values of ξ correspond to the maximum spread factor on a surface at room temperature and thus lead to an underestimation of the cooling rate j. Note also that the evaporation time Δt and the atomization volume ratio p could be accurately evaluated from the side-view images recorded by the high-speed camera; therefore, the top-view images recorded by the CCD camera should not be used for this purpose.

The corresponding results for the spread factor ξ and the cooling rate j are presented in Table 3. It is emphasized that the underestimated values of the cooling rate are close to or exceed the very large value of $j \approx 0.607$ kW/cm^2. It is worth noting that no clear dependence of j on the impact velocity is visible in Table 3.

3.5. Comparison of Drop Impacts and Cooling Rates for Copper-Plated, Silver-Plated, Nickel-Plated, and Gold-Plated Nanofiber Mats. Drop impact morphologies and the corresponding cooling rates through different metal-plated nanofiber mats (and a bare copper substrate used as a control) were studied at a fixed height of water drop release at $h = 17.95$ cm. The latter corresponds to the drop impact velocity of $V_0 = 187.66$ cm/s and the overestimated spread factor of $\xi = 3.407$. The fixed hot plate temperatures were chosen to be 125, 150, and 200 °C (display temperatures corresponding to 102.7, 125.6, and 172.2 °C for the sample, respectively). Drop impact morphologies at different metal-plated nanofiber mats are shown in Figures 10−12, which correspond to 125, 150, and 200 °C (the display temperatures), respectively. It is clearly seen that on all metal-plated nanofibers a drop of water fully evaporates faster than on the bare copper substrate used for control. Moreover, at higher temperatures of 150 and 200 °C (the display temperatures corresponding to 125.6 and 172.2 °C for the samples, respectively) the drop of water bounces back and levitates over the bare copper substrate, which corresponds to the Leidenfrost effect.

The comparison and discussion of the results for the different metal-plated nanofiber mats are facilitated by the values of the thermal diffusivities of these metals. According to ref 24, the values of the thermal diffusivity are as follows: for copper, $\alpha_{Cu} = 1.1$ cm^2/s; for silver, $\alpha_{Ag} = 1.7$ cm^2/s; for nickel, $\alpha_{Ni} = 0.19$ cm^2/s; and for gold, $\alpha_{Au} = 1.23$ cm^2/s. The most effective fibers yielding the fastest evaporation according to Figures 10−12 are the copper-plated fibers, with the silver-plated fibers being second and producing similar evaporation times. The highest efficiency of copper and silver could be expected on the basis of their high values of thermal diffusivity and highly developed thorny-devil-like or dendritelike roughness depicted for these fibers in Figures 2 (copper) and 3 (silver). The fact that the nickel-plated fibers lag behind the copper-plated and silver-plated ones is not surprising given an order-of-magnitude lower thermal diffusivity of nickel compared to that of copper and silver and the lower fiber roughness (cf. Figure 4 with Figures 2 and 3). The most striking fact visible in Figures 10−12 is that the gold-plated fibers lag far behind the copper-plated fibers, even though the thermal diffusivities of copper and gold are similar. The latter inevitably leads to the conclusion that thorny-devil-like copper-plated fibers are much more effective in drop cooling than the smooth gold-plated ones (cf. Figures 2 and 5) just because the surface area of the former is dramatically higher than that of the latter. It is emphasized that gold-plated nanofibers yield an evaporation time as long as that on the nickel-plated fibers (cf. Table 4), even though the disparity in the corresponding

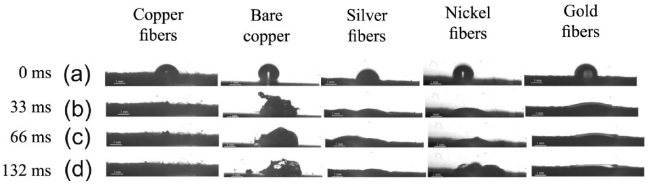

Figure 10. Drop impact onto thorny devil nanofibers at 125 °C (the display temperature corresponding to 102.7 °C for the samples). The five columns correspond (from left to right) to copper-plated fibers, a bare copper substrate, silver-plated fibers, nickel-plated fibers, and gold-plated fibers, respectively. The four rows (a−d) correspond to $t = 0$, 33, 66, and 132 ms, respectively.

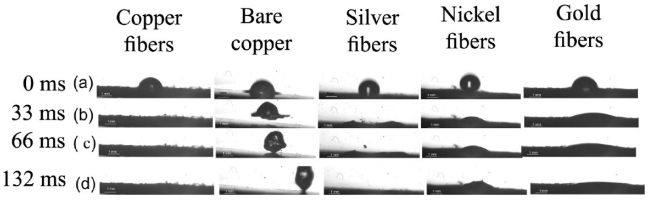

Figure 11. Drop impact onto thorny devil nanofibers at 150 °C (the display temperature corresponding to 125.6 °C for the samples). The five columns correspond (from left to right) to copper-plated fibers, a bare copper substrate, silver-plated fibers, nickel-plated fibers, and gold-plated fibers, respectively. The four rows (a−d) correspond to $t = 0$, 33, 66, and 132 ms, respectively. Note that the surface of the bare copper substrate looks as if it is inclined because illuminating makes a part of its surface too shiny and thus invisible. This is an optical artifact.

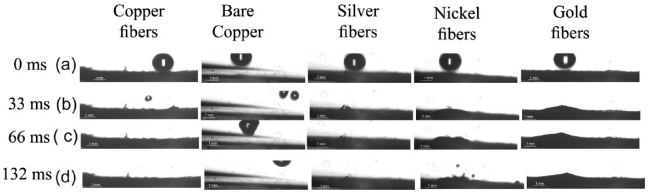

Figure 12. Drop impact onto thorny devil nanofibers at 200 °C (the display temperature corresponding to 172.2 °C for the samples). The five columns correspond (from left to right) to copper-plated fibers, a bare copper substrate, silver-plated fibers, nickel-plated fibers, and gold-plated fibers, respectively. The four rows (a−d) correspond to $t = 0$, 33, 66, and 132 ms, respectively.

(22) Scheller, B. L.; Bousfield, D. W. *AIChE J.* **1995**, *41*, 1357.
(23) Yarin, A. L. *Annu. Rev. Fluid Mech.* **2006**, *38*, 159.
(24) Rohsenow, W. M.; Hartnett, J. P.; Cho, Y. I. *Handbook of Heat Transfer*, 3rd ed.; McGraw-Hill: New York, 1998.

thermal diffusivities is on the order of 1 order of magnitude in favor of gold. It is also worth mentioning that the evaporation times on metal-plated nanofiber mats are dramatically shorter than those previously reported for the polymer mats.[6] In particular, the shortest evaporation times measured in the present work are about 400 times shorter than the shortest times reported in ref 6 for the comparable temperatures.

The results for the cooling rate j reported in Table 4 are based on the directly measured values of the loss fraction p evaluated from a careful analysis of the atomization during boiling using multiple video images similar to several frames depicted in Figures 13−16. The latter Figures also contain the measured values of p during the whole process and the final plateau value. For the copper-plated mats, the largest value of p does not exceed 0.1 (i.e., it is less than 10%, Figure 13). For the bare copper substrate, mass losses during boiling are quite dramatic, with p being on the order of 0.3 (Figure 14), which means that about 30% of the initial drop was atomized and lost. For the silver-plated nanofibers, maximum value of p is about 0.03 (relatively low losses, Figure 15); however, for the nickel-plated fibers, the losses might be as high as 20% (Figure 16). Note that there was no water atomization and thus no losses when boiling took place in gold-plated nanofiber mats.

The results for the cooling rate presented in Table 4 are based on the measured values of p. The nonzero values of p in Table 4 led to lower values of j for copper-plated fibers listed there compared to the case in Table 3 (probably because of sample-to-sample variability). Still, these values are close to the extremely high value of 0.4 kW/cm^2.

Table 4. Evaporation Times and Cooling Rates for Different Metal-Plated Nanofiber Mats and a Bare Copper Substrate[a]

material	temperature (°C)	Δt (ms)	p	j (kW/cm^2)
bare copper	125	264	0.27	0.256
	150	N/A	N/A	N/A
	200	N/A	N/A	N/A
copper nanofibers	125	172.5	0.04	0.136
	150	53	0.11	0.392
	200	52	0.09	0.408
silver nanofibers	125	170	0	0.138
	150	128.5	0.006	0.181
	200	55.5	0.03	0.407
nickel nanofibers	125	355	0.074	0.061
	150	600	0.20	0.031
	200	388	0.10	0.054
gold nanofibers	125	495	0	0.047
	150	633.5	0	0.037
	200	468	0	0.049

[a] For the bare copper substrate, the value of the spreading ratio used to calculate the corresponding heat flux j was measured directly from the top-view images.

4. Theoretical Evaluation of the Drop Evaporation Time on Nanofiber Mats and Discussion

In addition to measuring the evaporation time Δt of water drops inside metal-plated nanofiber mats, it is worth theoretically

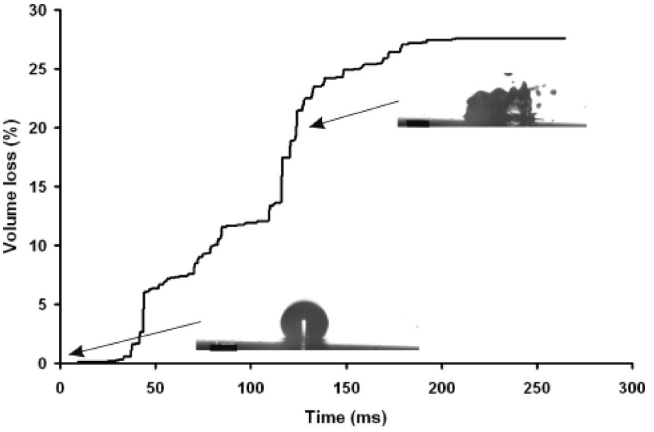

Figure 14. Mass losses due to atomization during the cooling of a bare copper substrate at 125 °C (the display temperature corresponding to 102.7 °C for the sample).

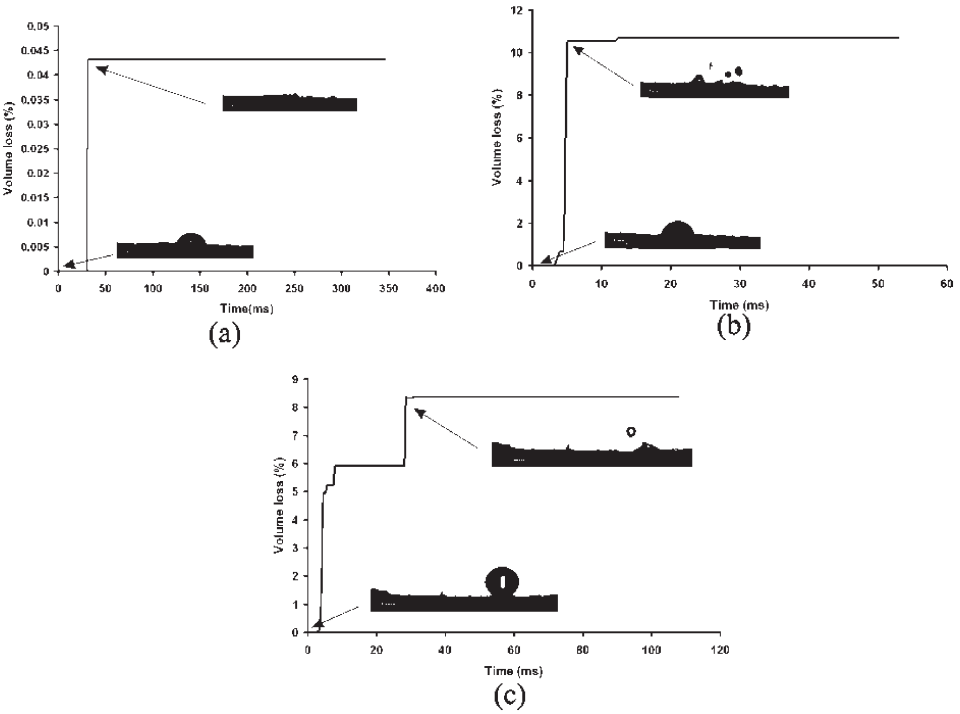

Figure 13. Mass losses due to atomization during cooling through copper-plated nanofiber mats. (a) 125, (b) 150, and (c) 200 °C (the display temperatures correspond to 102.7, 125.6, and 172.2 °C for the samples, respectively).

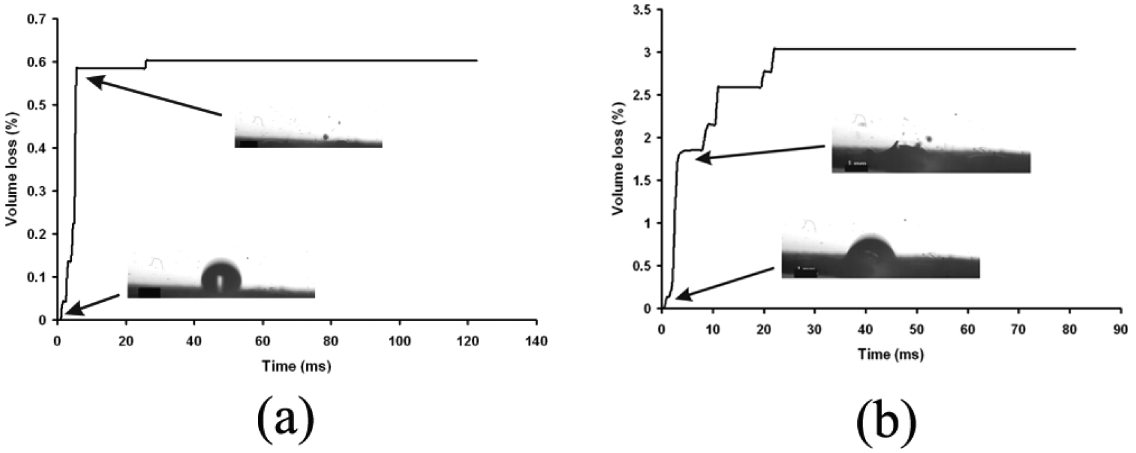

Figure 15. Mass losses due to atomization during cooling through silver-platted nanofiber mats. (a) 150 and (b) 200 °C (the display temperatures corresponding to 125.6 and 172.2 °C for the samples, respectively).

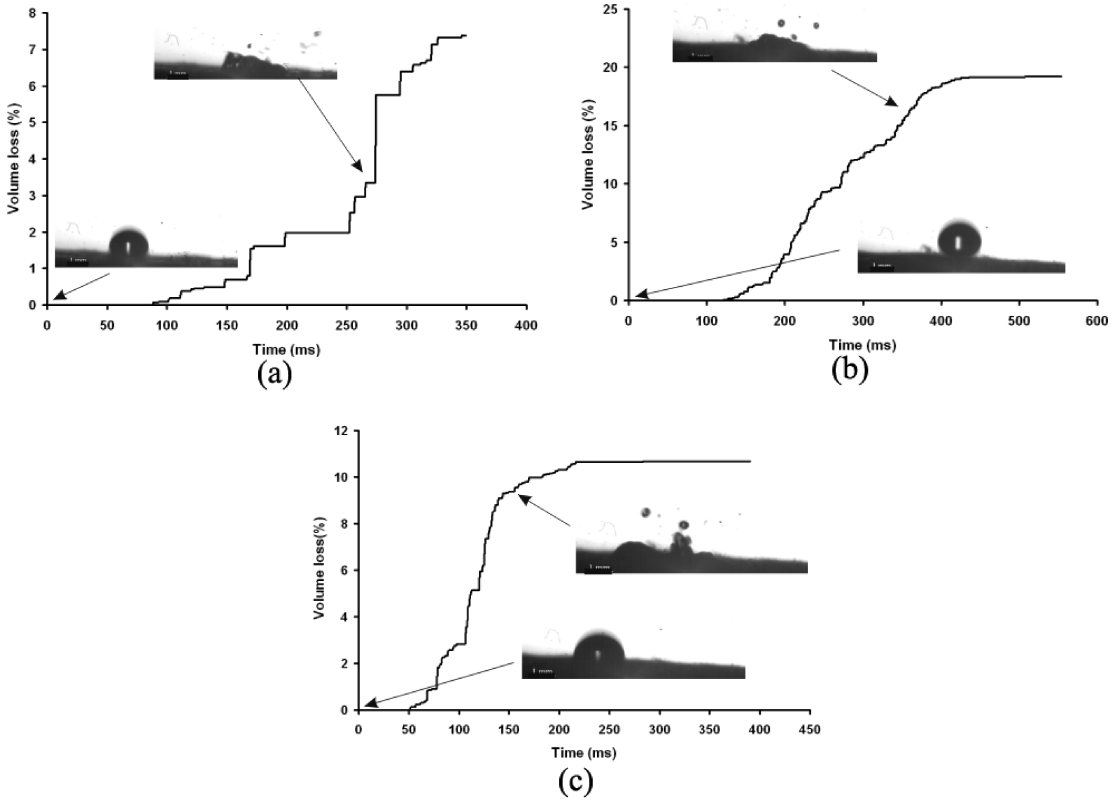

Figure 16. Mass losses due to atomization during cooling through nickel nanofiber mats. (a) 125, (b) 150, and (c) 200 °C (the display temperatures corresponding to 102.7, 125.6, and 172.2 °C for the samples, respectively).

estimating it for comparison with the data. That will allow the verification of the fact that complete evaporation inside nanofiber mats can happen at approximately the same moment when visible signs of the presence of water on the mat surface disappear. According to ref 25, we can expect that bubble nucleation responsible for evaporation happens predominantly at the nanofiber surfaces in contact with water in the pores instead of bulk evaporation inside the body of water in the pores. When evaporation into a vapor embryo begins, the embryo practically contains only air (and no vapor) and vapor concentration c inside it might be described in the first approximation by the self-similar distribution near a plane surface

$$\frac{c}{c_s(T)} = 1 - \mathrm{erf}\left(\frac{y}{2\sqrt{Dt}}\right) \quad (6)$$

where $c_s(T)$ is the saturated vapor concentration near a liquid/vapor interface inside the embryo determined by the current local temperature T, y is the distance from the interface (with larger values of y, in fact, corresponding to the embryo center), D is the diffusion coefficient of vapor, and t is time.

In the almost flashlike evaporation that we are dealing with inside the pores in the metal-plated nanofiber mats, vapor bubbles almost instantaneously fill the whole pore. Therefore, their size

(25) Kenning, D. B. R. In *Two-Phase Flow and Heat Transfer*; Butterworth, D., Hewitt, G. F., Eds.; Oxford University Press: Oxford, U.K., 1977.

can be taken as the pore size δ. According to eq 6, the vapor mass flux into a vapor embryo is then equal to

$$\dot{M} = \delta^2 c_s(T)\sqrt{\frac{D}{\pi t}} \tag{7}$$

Using the Clapeyron equation and the equation of state (assuming the vapor to behave as an ideal gas), we find that

$$c_s(T) = k_0 \exp\left(-\frac{E}{RT}\right) \tag{8}$$

where R is the absolute gas constant and

$$E = L\mu_m,\ k_0 = \frac{p_{s_0}\mu_m}{RT_w}\exp\left(\frac{E}{RT_0}\right) \tag{9}$$

In the latter equations, μ_m is the molecular weight of vapor, p_{s_0} is the saturated vapor pressure at temperature T_0, and T_w is the substrate temperature, which is assumed to be equal to the metal-plated nanofiber temperature. Equation 9 shows that E plays the role of the evaporation activation energy and k_0 is a pre-exponential factor.

The average magnitude of the heat removal rate as a latent heat of evaporation in a pore during the characteristic evaporation time Δt is equal to

$$\dot{Q}_I = L\frac{1}{\Delta t}\int_0^{\Delta t}\dot{M}\,dt \tag{10}$$

Using eqs 7−9, we find that the latter yields

$$\dot{Q}_I = A\exp\left(-\frac{E}{RT}\right) \tag{11}$$

where the pre-exponential factor is given by

$$A = \frac{2L\delta^2\mu_m}{RT_w}\,p_{s_0}\exp\left(\frac{E}{RT_0}\right)\sqrt{\frac{D}{\pi\Delta t}} \tag{12}$$

However, heat is supplied through a metal substrate plate (wall) to the nanofiber mat attached to it and thus to water in the pore by thermal conduction. The corresponding heat flux is

$$\dot{Q}_{II} = \frac{k_w}{\delta_w}(T_w - T)\delta^2 \tag{13}$$

In a zero-dimensional model,[26] the equality

$$\dot{Q}_I = \dot{Q}_{II} \tag{14}$$

determines the evaporation temperature T_{ev}. According to eqs 11, 13, and 14, it can be found from the following equation that

$$A\exp\left(-\frac{E}{RT_{ev}}\right) = \frac{k_w}{\delta_w}(T_w - T_{ev})\delta^2 \tag{15}$$

However, the evaporation time Δt is evaluated as

$$\Delta t = \frac{\rho\delta^3}{(A/L)\exp(-E/RT_{ev})} \tag{16}$$

where ρ is the liquid (water) density.

By substituting eq 12 in eq 16, we arrive at

$$\Delta t = \frac{\pi}{D}\left\{\frac{\rho\delta RT_w\exp[E(T_{ev}^{-1} - T_w^{-1})/R]}{2\mu_m p_{sw}}\right\}^2 \tag{17}$$

where p_{sw} is the vapor pressure at the substrate temperature T_w.

It is emphasized that T_{ev} on the right-hand side of eq 17 depends on Δt through eqs 12 and 15. Therefore, eq 17 is a highly nonlinear equation for Δt. A significant simplification, however, is possible. Namely, it is possible to show using the Frank−Kamenetskii transformation familiar from combustion theory[26] that when the inequality

$$\frac{(k_w/\delta_w)R^2T_w^3}{2E^2p_{sw}[D/(\pi\Delta t)]^{1/2}} \gg 1 \tag{18}$$

holds, the temperature $T_{ev} \approx T_w$, and eq 17 reduces to the following expression for the evaporation time Δt

$$\Delta t = \frac{\pi}{D}\left(\frac{\rho\delta RT_w}{2\mu_m p_{sw}}\right)^2 \tag{19}$$

Taking for the estimate $\rho = 1$ g/cm^3, the pore size $\delta = 10^{-4}$ cm, $T_w = 373$ K, $\mu_m = 18$ g/mol, and $D = 0.21$ cm^2/s and using the standard expression for the saturation pressure of water as a function of temperature to evaluate p_{sw} from refs 27 and 28, we find from eq 19 that $\Delta t = 0.11$ s. Then, we check a posteriori that the left-hand side of eq 18 is equal to 5.4×10^6 for a wall composed of copper nanofibers (i.e., the inequality (eq 18) indeed holds).

It is emphasized that the predicted value of Δt on the order of 100 ms is close to the values of the evaporation time measured experimentally for copper and silver nanofiber mats, which are listed in Tables 3 and 4. The agreement between the predicted and measured values corroborates the latter ones and supports the conclusion based on processing the experimental data in the Experimental Section that cooling rates in the range of 0.4−0.6 kW/cm^2 were achieved using such nanofiber mats.

5. Conclusions

A new method of electroplating electrospun nanofiber mats allowed us to prepare copper-, silver-, nickel-, and gold-plated mats. The copper- and silver-plated individual nanofibers revealed high surface roughnesses, which made them similar to thorny devil lizards and dendrites/cactuses, respectively. In addition, these nanofibers and their mats possess high thermal diffusivities.

Copper substrates with deposited metal-plated nanofiber mats with thicknesses of about 30 μm were heated to constant temperatures of up to 172 °C, and single water drop impacts on them were used for localized cooling. The results reveal the following. The presence of nanofiber mats dramatically reduces water losses due to boiling-associated atomization (zero or several percent loss on copper-plated nanofiber mats on a copper substrate compared to about 30% on a bare copper substrate). Moreover, the presence of nanofiber mats completely eliminated drop bouncing characteristic of bare hot surfaces (i.e., suppressed the Leidenfrost effect). It was shown that nanofiber surface roughness plays a more significant role than its thermal diffusivity in the enhancement of the drop evaporation rate and thus the heat removal rate. As a result, with copper-plated nanofiber mats, cooling rates close to 0.6 kW/cm^2 were demonstrated, which is an impressive value in comparison with the previously achieved values reported in the literature. The experimentally measured evaporation times on

(26) Zeldovich, Ya.B.; Barenblatt, G. I.; Librovich, V. B.; Makhviladze, G. M. *The Mathematical Theory of Combustion and Explosions*; Consultants Bureau: New York, 1985.

(27) Seaver, M.; Galloway, A.; Manuccia, T. J. *Rev. Sci. Instrum.* **1989**, *60*, 3452.

(28) Yarin, A. L.; Brenn, G.; Kastner, O.; Rensink, D.; Tropea, C. *J. Fluid Mech.* **1999**, *399*, 151.

metal-plated nanofiber mats were supported by the theoretical estimates.

Acknowledgment. Partial support of this work by the NSF (grant CBET 0966764) and NASA (grant NNX10AR99G) is greatly appreciated. The help of two undergraduate students, Y. Chan (an NSF REU summer fellow) and F. Charbel, with data processing is gratefully acknowledged.

Appendix I: Electroplating of Copper

For the electroplating of copper, sulfuric acid was added to the electroplating bath to improve the conductivity and process efficiency, which also could prevent the formation of the oxide layers. During the electroplating process, copper is dissolved at the anode with the participation of sulfuric acid, and the copper anode is in solubility equilibrium with the dissolved $CuSO_4$. Copper is lost from the electrolyte during electroplating and can be replaced by copper dissolved from the anode. Therefore, copper concentration in the electrolyte should be constant during the electroplating process. In this process, not only Cu^{2+} but also Cu^{+} ions will be dissolved from the anode material. After the deposition was over, the electrodes and the electrolyte were stored separately from each other to avoid any change in the electrolyte copper concentration in future electroplating on nanofibers. For the copper sulfuric electroplating bath used in this work, the redox reactions were as follows:

$$\text{cathode}: \ Cu^{2+} + 2e^- \rightarrow Cu \qquad \text{(AI.1)}$$

$$\text{anode}: \ Cu \rightarrow 2e^- + Cu^{2+} \qquad \text{(AI.2)}$$

Appendix II: Electroplating of Silver

For silver electroplating in this work, the following reactions took place in the electroplating bath:

$$AgNO_3 + KOH \rightarrow AgOH + KNO_3 \qquad \text{(AII.1)}$$

$$AgOH + 2NH_3 \rightarrow [Ag(NH_3)_2]^+ + OH^- \ \text{(Tollen's Reagent)} \qquad \text{(AII.2)}$$

$$\text{cathode}: \ [Ag(NH_3)_2]^+ + e^- \rightarrow Ag + 2NH_3(aq) \qquad \text{(AII.3)}$$

$$\text{anode}: \ Ag \rightarrow e^- + Ag^+ \qquad \text{(AII.4)}$$

Appendix III: Electroplating of Nickel

For nickel electroplating using nickel sulfamate, the following redox reactions took place in the electroplating bath:

$$\text{cathode}: \ Ni^{2+} + 2e^- \rightarrow Ni \qquad \text{(AIII.1)}$$

$$\text{anode}: \ Ni \rightarrow 2e^- + Ni^{2+} \qquad \text{(AIII.2)}$$

Appendix IV: Electroplating of Gold

For the gold plating, the following reactions were implemented in the electroplating bath:

$$SO_3^{2-} + 2OH^- \rightarrow SO_4^{2-} + H_2O + 2e^- \qquad \text{(AIV.1)}$$

$$AuCl_4^- + 2e^- \rightarrow AuCl_2^- + 2Cl^- \qquad \text{(AIV.2)}$$

$$AuCl_2^- + 2SO_3^{2-} \rightarrow [Au(SO_3)_2]^{3-} + 2Cl^- \qquad \text{(AIV.3)}$$

The overall reaction was

$$AuCl_4^- + 3SO_3^{2-} + 2OH^- \rightarrow [Au(SO_3)_2]^{3-} + 4Cl^- + SO_4^{2-} + H_2O \qquad \text{(AIV.4)}$$

and the redox reactions were

$$\text{cathode}: \ AuCl_4^- + 3e^- \rightarrow Au + 4Cl^- \qquad \text{(AIV.5)}$$

$$\text{anode}: \ Au \rightarrow 3e^- + Au^{3+} \qquad \text{(AIV.6)}$$